Results in Physics 8 (2018) 422–428

Contents lists available at ScienceDirect

Results in Physics

journal homepage: www.journals.elsevier.com/results-in-physics

Investigation of the percentage and the compacting pressure effect on the structural, optical and thermal properties of alumina-zeolite mixture

C. Messaadi [a,c], T. Ghrib [b,*], M. Ghrib [a], A.L. Al-Otaibi [b], M. Glid [c], H. Ezzaouia [a]

[a] Laboratory of Semiconductor Nanostructures and Advanced Technologies, Research and Technologies Center of Energy, Borj Cedria, Tunisia
[b] Department of Physics, College of Science of Dammam, Imam Abdulrahman Bin Faisal University, P. O. 383, Dammam 31113, Saudi Arabia
[c] Science Faculty of Bizert, University of Carthage, Tunisia

ARTICLE INFO

Article history:
Received 27 June 2017
Received in revised form 12 November 2017
Accepted 17 December 2017
Available online 19 December 2017

Keywords:
NaA zeolite
Alumina
Photoluminescence
Thermal properties

ABSTRACT

This paper presents a detailed investigation of the correlation between micro-structural, optical and thermal properties of a mixture constituted of NaA zeolite and Al_2O_3 alumina with different portions at various compacting pressures. A comprehensive study was made by using SEM, EDX, XRD, PL and PTD analysis. Through this full characterization, it was demonstrated that a mixture of grain size ranging from 50 nm to 85 nm can be used as a red emitter of mean wave length $\lambda = 650$ µm in optical devices. This mixture also proved to be used as a thermoinsultor or a thermocondensor material; with a thermal conductivity of about 0.22–1.33 $W{\cdot}m^{-1}{\cdot}K^{-1}$ and a thermal diffusivity of about 0.070–0.174 $cm^2{\cdot}s^{-1}$.

Introduction

Zeolites are microporous, alumino silicate minerals, consisting of three-dimensional arrangement of SiO_4 and Al_2O_3, linked by oxygen atoms that form different construction units and large frameworks. Having specific nanochannels, nanopores and ion-exchange capacity, zeolites can be used in various applications as molecular sieves, adsorbents, catalysts [1]. The synthesis of zeolites, has received significant attention in recent years. This is because they have a wide variety of starting materials containing high amounts of Si and Al, e.g., kaolin, high-silica bauxite, halloy site, interstratified illitesmectite, montmorillonite...etc. [2–9]. Zeolites were confined almost 200 years ago in mineralogical museums because of their beauty. The ability to synthesize with a controlled structure and size also proved to be useful in various applications ranging from the separation gas catalytic processes in petroleum refining [10,11]. However, researches dedicated to the synthesis of zeolites remain extremely teeming, as evidenced by the number of studies related to synthetic zeolites compared to those naturals.

Several researchers reported that the alumina used as templates for nanosize structures such as optoelectronic devices [12,13], magnetic storage [14], solar cells [15], carbon nanotubes [16], catalysts [17] and metal nanowires [18,19]. The investigation of the thermal properties is useful in understanding the structural evolution of some components against internal and external effects. In this regard, Somayajulu [20] presented a study of pellets of ThO_2-CeO_2 mixed oxide (MOX). A combined experimental and theoretical methodology was used in that research which helped determine the thermo-physical properties such as elastic modulus, specific heat, thermal expansion and thermal conductivity. Those properties were then compared with respect to homogeneity, microstructure, porosity and oxygen to metal ratio.

The effect of surface modification of 4A zeolite on physical and electrical properties of copolyimide hybrid films was investigated by Biçen et al. [21]. They demonstrated that that effect contributed to thermal, mechanical and hydrophobicity properties. The thermal conductivity of evacuated packed powders of zeolite NaX was investigated as a function of particle size and temperature by Jakubinek et al. [22]. They showed that particles of 2 mm and 800 nm had a temperature in the range of 5–400 K and that their thermal conductivity varied in the range of 0.0025–0.17 $W{\cdot}m^{-1}{\cdot}K^{-1}$.

This paper presents a detailed investigation and correlation between microstructural, optical and thermal properties using new strategy applied to a mixture of NaA zeolite and Al_2O_3 alumina powder denoted NaA/Al_2O_3. The NaA/Al_2O_3 mixture was systematically studied by scanning electron microscopy (SEM), X-ray diffraction (XRD) and the energy dispersive X-ray (EDX) to check the purity phase, structure and grain size of the powder. The photoluminescence (PL) response was also found versus the mass

* Corresponding author.
E-mail address: taher.ghrib@yahoo.fr (T. Ghrib).

https://doi.org/10.1016/j.rinp.2017.12.048
2211-3797/

proportion in the mixture. That powder was manufactured; in the form of pellets with different compacting pressures for two different mass percentages of the mixture, and after that it was restudied. The thermal properties were determined by means of the photothermal deflection (PTD) technique [23–27]; which is a non-destructive technique and sensitive to any fine physical and structural changes of all types of materials.

Method and microstructural characterization

The NaA zeolite was synthesized by methods known in the ref [28] by using a well natural kaolinite from Tamra mine (HI = 1.23) in the north of Tunisia (KTM). This kaolin material was hydrothermally digested by NaOH and leached with dilute HCl. This gave an acid solution which would be adjusted by NaOH in order to precipitate an amorphous Si and an Al white gel with a proper ratio of Al/Si, which was then used for the NaA zeolite synthesis. This white gel would be dissolved in 1.0 M NaOH and crystallized at 90 °C in a stainless steel autoclave for 3 days. A solid product obtained, filtered out, washed with deionized water, and dried at 90 °C for about 10 h, constituted the A zeolite.

The study developed two sets of samples in the form of pellets constituted by a mixture of NaA zeolite and Al_2O_3 alumina with two different percentages A($m_{zeo} = \frac{1}{5} m_{alumin}$) and E($m_{alumin} = \frac{1}{5} m_{zeo}$) at three different compacting pressures which are detailed in Table 1.

In order to determine the structure of the specimens, the samples were characterized by powder XRD analysis performed with a D8 Bruker AXS powder diffractometer. The X Powder analytical software was used for the semi-quantitative determination of the mineral phases by an automated processing of the diffraction data. The studies were carried out using Cu Kα radiation of wavelength $\lambda = 1.540$ Å in a 2θ range of 5–45°. Fig. 1 shows the XRD pattern of the pure synthesized NaA zeolite and the two mixtures: A and E. In all the three curves the peaks (2 2 2), (4 4 0), (4 2 2), (4 4 2), (6 4 2), (6 4 4), and (6 6 4) appear respectively at 2θ = 9.17°, 18.34°, 22.22°, 23.81°, 27.83°, 29.04° and 33.93° are characteristic of zeolite-A (NaA) with a chemical composition: $Na_{12}(Al_{12}Si_{12})O_{48}.(H_2O)_{18}$ which are in good agreement with the results obtained by Reed, Gramlich, Simmen and Zivica et al. [29–32]. It is worth noting that the obtained peaks are of different intensities and widths which indicate that this product is an amorphous material. According to those peaks the grain sizes δ were determined using respectively Bragg's law and Debye Scherer's method of equation:

$$\delta = \frac{1.2\lambda}{\Delta(2\theta)\cos\theta}$$

where Δ(2θ) is the value of the full width at half maximum (FWHM) of these peaks. This calculation shows that the grain size is from 50 nm to 5 μm. The study of the XRD pattern A and E shows the emergence of new peaks (2 2 0), (4 2 0), (5 5 5) and (8 4 0) respectively at 2θ = 7.27°, 12.66°, 31.03° and 33.04° which are related to the structure alumina inserted in the zeolite matrix (curve A) or that of the zeolite inserted in the alumina matrix (curve E) from which it is reclaimed that the mixture is an insertion mutation and it is also

Table 1
Samples and its concentrations and compacting pressures.

Samples	Compacting pressure (10^3 torr)
$A \ldots \rightarrow \boldsymbol{m_{zeo} = \frac{1}{5} m_{alumin}}$	$3 \ldots \rightarrow 30$
$E \ldots \rightarrow \boldsymbol{m_{alumin} = \frac{1}{5} m_{zeo}}$	$4 \ldots \rightarrow 40$
	$5 \ldots \rightarrow 50$
Example:$A3\,(\boldsymbol{m_{zeo} = \frac{1}{5} m_{alumin}}) - \rightarrow$ with 30 ktorr of compacting pressure	

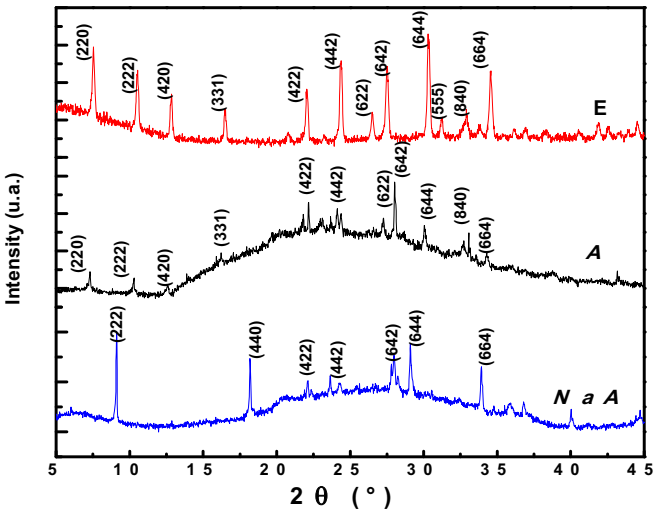

Fig. 1. X-ray powder diffraction pattern of NaA zeolite and A and E zeolite-alumina mixtures.

deduced by studying the peaks of the two latter curves and that the grains of the E-mixture are softer than that of the A one.

The morphological features were determined by the FEI Quanta 200 scanning electron microscope, equipped with an energy dispersive X-ray (EDX) analyzer. Analyses were performed in up to five different areas of each sample by continuous raster scanning at 25 kV. Fig. 2 shows microstructures of the initial NaA zeolite as deduced from SEM and EDX experiments. The SEM micrographs show particles of a partially deformed spherical shape with various sizes provided of pores indicating an amorphous and non compacting structure. The presence of the main elements O, Na, Al, Si and other minor elements can be seen in the EDX spectrum which identifies the metakaolin recognized by Zivica et al. [32] and Meftah et al. [28] which is used in this work as a starting material for the preparation of the zeolite sample.

The SEM and EDX analyses of these A and E mixtures are given in Fig. 3 for the same compacting pressure equal to 40 kilo-torr; from which it is denoted that the matrix of A-mixture has more pores than that of the E-mixture which indicated that the latter is more compacted than that of the A one. This behavior may be related to the Al_2O_3 grain size whose value is in the order of 0.5–2.2 μm of the same order of that they obtained by XRD analysis of Fig. 1 and those obtained by Pham et al. [33]; whose obtained Al_2O_3 composite of grain size was in the order of 0.5–1.1 μm. The effect on the structure, optical and thermal properties of the NaA/Al_2O_3 mixture are studied and detailed below.

Photoluminescence properties

Fig. 4a and b show the PL spectrum in the UV–visible range and in the spectral range from 500 to 800 nm of the pure alumina Al_2O_3 and NaA zeolite materials and the NaA/Al_2O_3 mixture for the two different percentages and with the three different compacting pressures. It is denoted that the comparison of the spectrum for the same compacting pressure, shows a displacement of the peak initially existing at about 780 nm for the pure NaA zeolite by a blue shift in the order of 130 nm for the three components and the two compacting pressures to become centered at $\lambda = 650$ μm showing that NaA/Al_2O_3 mixture can be used as red emitter in optical devices. Furthermore, this observed PL shift may be related to the recombination of electrons in the conduction band and holes in the valence band of semi conductors. This requires an enlargement of the band gap especially for quantum confinement or the

EDX Quantification

Elem	wt%	at%
O	29.80	41.6
Na	9.01	8.76
Al	28.60	23.69
Si	32.59	25.93

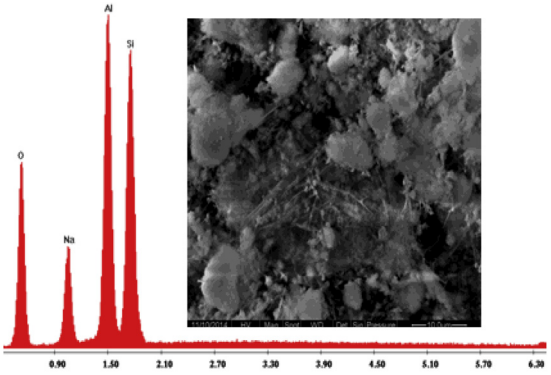

Fig. 2. EDX and SEM micrographs of synthesized NaA zeolite.

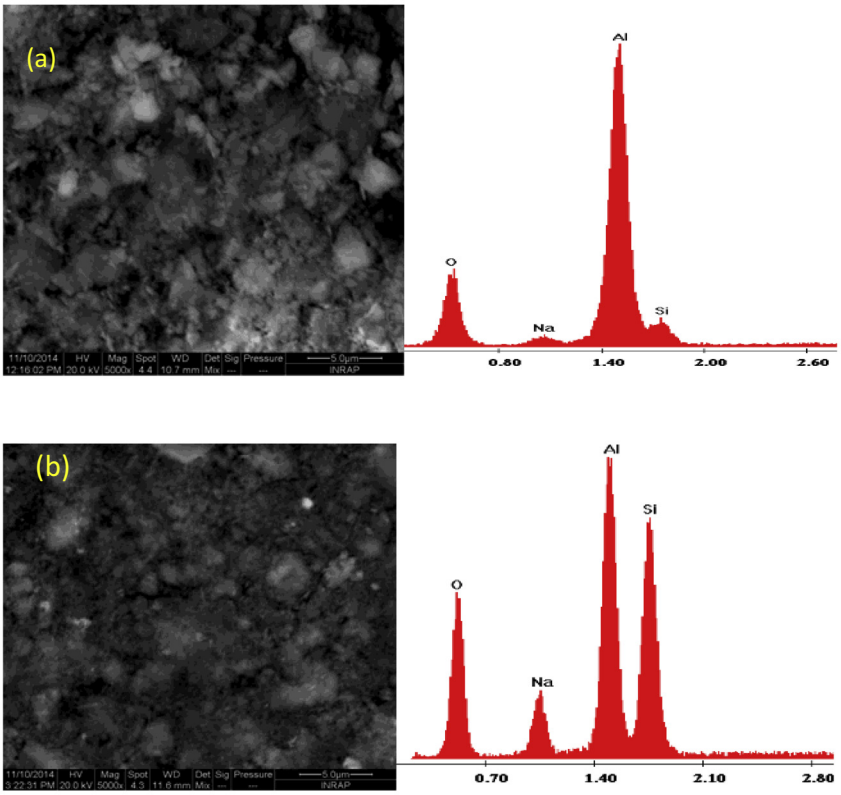

Fig. 3. EDX and SEM micrograph of synthesized mixtures A_4 (a) and E_4 (b).

inter-band transition related to Si–O/Si–H ratio which decreases by increasing the alumina mass in the mixture. Then it can be deduced that this behavior does not seem to have its origin only from the zeolite embedded in the porous alumina matrix or the converse but it is due to the contributions of the two materials. Fig. 3 shows the SEM images which confirm that the prepared powder is constituted of big grains of micrometric size which are internally filled with small grains of dimensions in the order of 50 nm or smaller. As indicated by the XRD study and the EDX spectrum, the variation of the Si-O percentage decreases versus the alumina portion causing an oxygen saturation and a reduction in the Si–O portion; which influence the Si–O/Si–H ratio and the PL spectra. This means in practice, that the compacting pressure does not have a remarkable influence in the PL emission which was expected from the beginning since the pressure cannot influence the electrical and optical properties of the material.

Thermal properties

The thermal conductivity, thermal diffusivity and heat capacity of materials can be measured by using the PTD technique. This technique, whose principle is given in Fig. 5, consists of heating the sample by a modulated light of intensity $I = I_0(1 + \cos \omega t)$ which will be absorbed on the sample surface and generate a thermal wave. This thermal wave will propagate in the sample and in the air surrounding it and will induce a temperature gradient and then a refractive index gradient in the fluid. The fluid index gradient will cause the deflection ψ of a probe laser beam skimming the

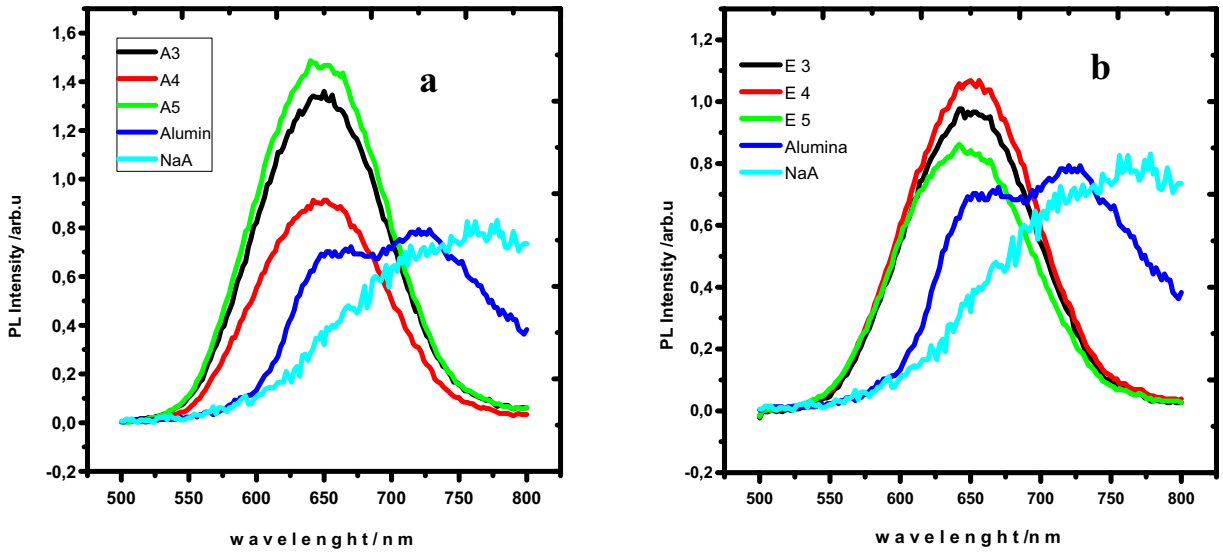

Fig. 4. Photoluminescence spectra of the mixtures (NaA/Al_2O_3) with various percentages.

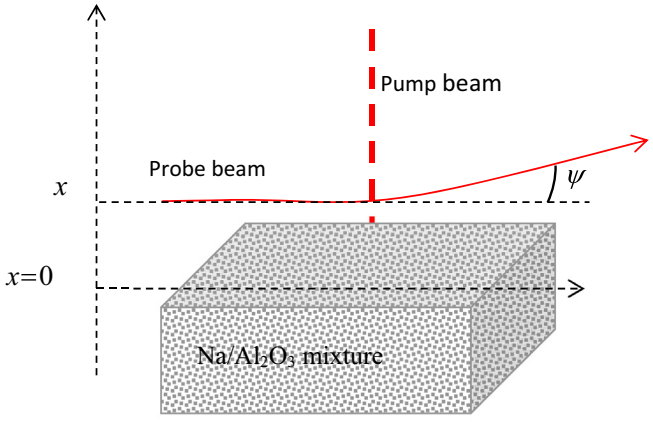

Fig. 5. Schema of the deflected probe beam on the sample surface.

sample surface (Fig. 6). This deflection may be related to the sample's thermal properties. The heating source is a halogen lamp of Power 100 W whose light is modulated by using a mechanical chopper with variable frequency. An (He-Ne) laser beam skimming the sample surface at a distance x is deflected. This deflection can be detected by a four quadrant photo-detectors and converted to an electrical signal which is measured by a lock-in amplifier. Through an intermediary interface between a mechanical chopper, a Look-in amplifier and a microcomputer the amplitude and phase of the photo-thermal signal will be measured and drawn according to the square root modulation frequency.

The amplitude $|\psi|$ and phase φ of the probe beam deflection ψ are given by [24]:

$$|\psi| = \frac{\sqrt{2}L}{n\mu_f}\frac{dn}{dT_f}|T_0|e^{-\frac{x}{\mu_f}} \text{ and } \varphi = -\frac{x}{\mu_f} + \theta + \frac{5\pi}{4}$$

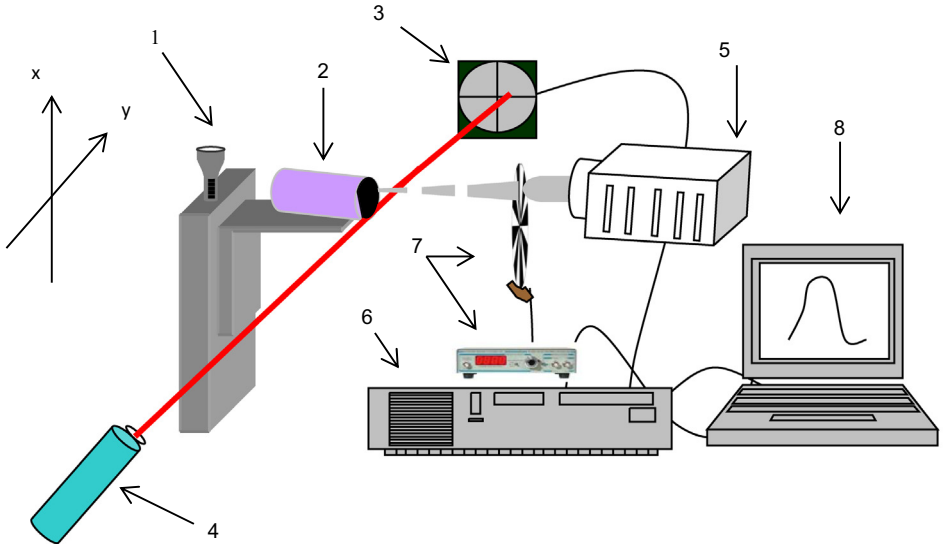

Fig. 6. Experimental set-up used for PTD investigation: 1-Table of micrometric displacement, 2-Sample, 3-Photodetector position, 4-Fixed laser source, 5-Halogen lamp, 6-Look-in amplifier, 7-Mechanical chopper, 8-Computer.

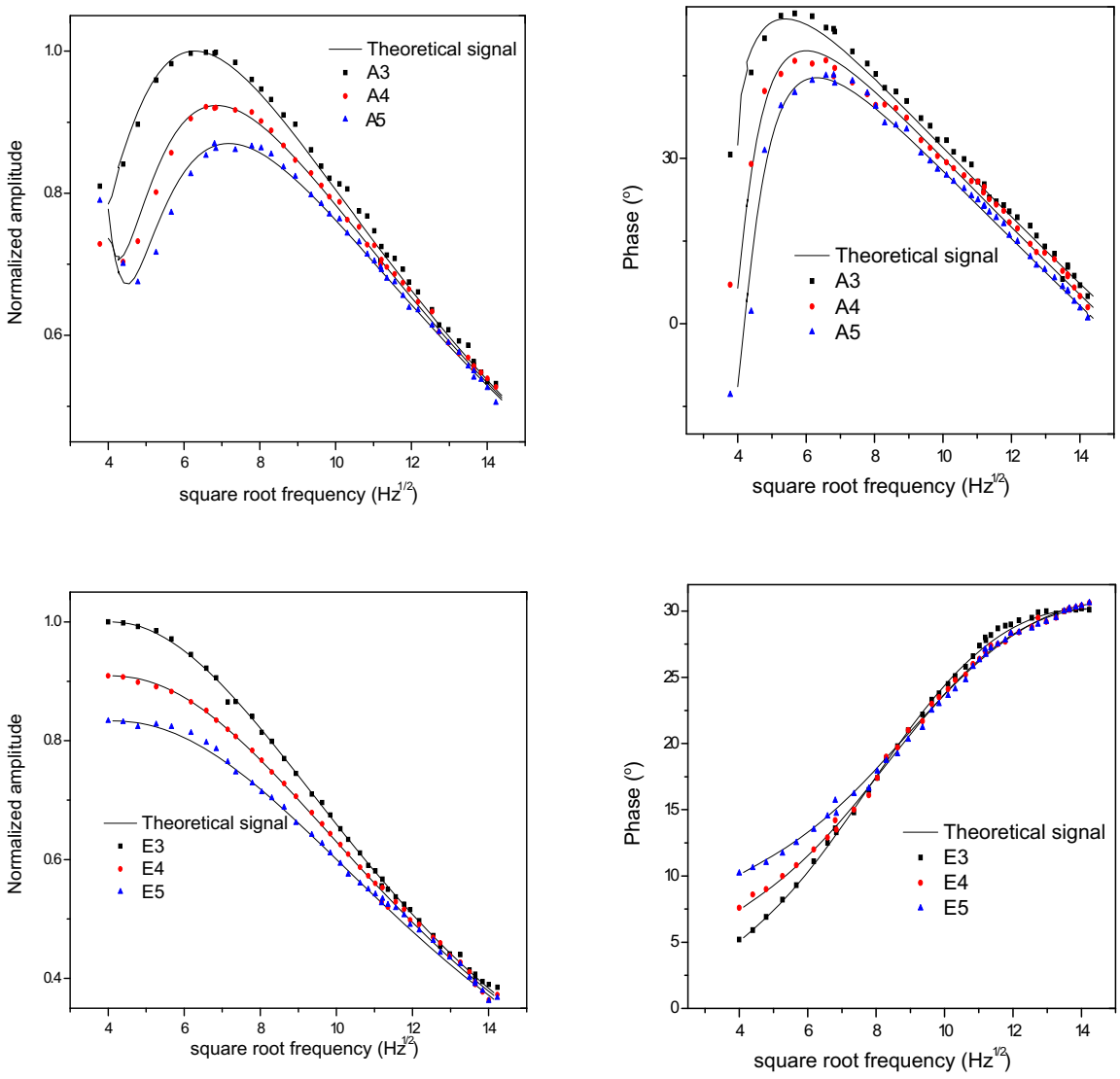

Fig. 7. Evolution of the thermal conductivity and thermal diffusivity of NaA/Al_2O_3 mixture.

Table 2
Thermal properties of the zeolithe NaA for various concentrations and compacting pressures.

Thermal properties	A_3	A_4	A_5	E_3	E_4	E_3
Thermal conductivity ($W{\cdot}m^{-1}{\cdot}K^{-1}$)	1.10	1.24	1.33	0.22	0.26	0.29
Thermal diffusivity ($cm^2{\cdot}s^{-1}$)	0.150	0.165	0.174	0.070	0.081	0.087
Heat capacity ($10^4\,J{\cdot}m^{-3}{\cdot}K^{-1}$)	7.33	7.55	7.64	3.14	3.21	3.33
Mean free path (nm)	22.50	24.75	51.10	10.50	12.15	13.05

where L is the width of the pump beam in the direction of the probe laser beam, n, μ_f and T_f are respectively the refractive index, the thermal diffusion length and the temperature of the fluid.

$|T_0|$ and θ are respectively the amplitude and phase of the surface temperature T_0 given by the formula:

$$T_0 = -E[(1-r)(1+b)e^{\sigma_s l_s} - (1+r)(1-b)e^{-\sigma_s l_s} + 2(r-b)e^{-\alpha l_s}]/[(1+g)(1+b)e^{\sigma_s l_s} - (1-g)(1-b)e^{-\sigma_s l_s}]$$

With $E = \frac{A}{\alpha^2-\sigma_s^2} = \frac{\alpha I_0}{2K_s(\alpha^2-\sigma_s^2)}$, $\sigma_s = (1+j)\sqrt{\frac{\pi f}{D_s}}$, $b = \frac{K_b\sigma_b}{K_s\sigma_s}$, $g = \frac{K_f\sigma_f}{K_s\sigma_s}$ and $r = \frac{\alpha}{\sigma_s}$

It can be noticed that these expressions are function of the sample's thermal properties and the modulation frequency.

The comparison of the experimental curve with its corresponding theoretical study gives the thermal conductivity and diffusivity of the sample. The experimental and theoretical variations of the amplitude and phase of the photothermal signal for the two sets are given in Fig. 7.

After the simulation, the obtained values are given in Table 2 for the different samples, in which it is denoted that both thermal conductivity and thermal diffusivity decrease with the compacting pressure and the alumina percentage for the same set. From these obtained thermal properties it is clear that the thermal conductivity decrease with the compacting pressure for the same alumina percentage and decrease with the alumina percentage with the same compacting pressure; which are in the same order of those obtained by Vladimir et al. [34] who studied the effective thermal

conductivity of dehydrated powdered 4A zeolite with the temperature and they obtained values in the order of 0.14 $W{\cdot}m^{-1}{\cdot}K^{-1}$ at room temperature. They are also in good agreement with the alumina prepared by Pedro et al. [35] who studied the pore size effect on the thermal conductivity of alumina foams and concluded that the mean value of the thermal conductivity was in the order of 0.8–1 $W{\cdot}m^{-1}{\cdot}K^{-1}$ at room temperature and would be more relevant for a low porosity density. The rise of the compacting pressure will decrease the pores volume and subsequently increase the thermal conductivity. On another hand, these small values suggest more general explanations. For instance, the internal vibration and thermal conduction are a result of optical phonons; which generally decrease with the grain size, and the porosity of powder materials; which play a relevant role to enhance the phonic heat conduction compared to the electronic one. In the application field, the material's low thermal conductivities values allow using it as a thermal insulator in micro-sensors. This can be supported by the research conducted by Fukushima et al. [36] which studied the preparation of highly porous mullite thermal insulators by gelation freezing route with a thermal conductivity ranging from 0.23 to 0.38 $W{\cdot}m^{-1}{\cdot}K^{-1}$ at room temperature.

According to the kinetic theory, the phonons mean free path is related to the thermal diffusivity D by $\lambda = 3D/v$, where v is the phonon group velocity, and can be calculated by using the determined thermal diffusivity. This mean free path is given in Table 2, according to the dispersion calculations which prove that the average phonon velocity in Zeolite is estimated at approximately 2000 m/s at 300 K [37]. The values of this mean free path decrease from 22.50 to 51.10 nm and from 10.50 to 13.05 nm with the compacting pressure respectively for the two mixtures A and E; which are in the order of the mean grain size, as shown before by using the XRD and SEM techniques.

In a general way, this means free path can be related to the internal vacuum rate λ_v, the crystal lattice λ_l and the crystalline defects λ_c of the sample by: $\frac{1}{\lambda} = \frac{1}{\lambda_v} + \frac{1}{\lambda_l} + \frac{1}{\lambda_c}$

It is important to mention the difference between the alumina and the zeolite being in the effect of Al atoms incorporation which are more voluminous than those of Si atoms and also have more free electrons. These influence the internal vacuum and the interatomic bonds like those of the Al-O which are more softer than those the Si-O causing a local enhancement in the vibration between atoms in the alumina structure compared to that of the zeolite and, consequently, an enhancement in the velocity propagation of heat inside the material; implying an increase of the thermal diffusivity. The compacting pressure increases the mean free path for the two mixtures which may be explained by the decrease in the vacuum density, the crystal lattice and the scattering defects; making an improvement in the heat conduction. All these thermal properties can be explained by the fact that the manufactured zeolite-alumina mixture can be used as a thermoinsultor or a thermocondensor material.

Conclusion

This work investigates alumina-zeolite mixture, describes the preparation method which is accurately used and studies the effect of the alumina/zeolite ratio and compacting pressures on the structure, PL emission and thermal properties. It is denoted that these mixtures have thermal conductivity, thermal diffusivity and mean free path respectively in the order of 0.22–1.33 $W{\cdot}m^{-1}{\cdot}K^{-1}$, 0.070–0.174 $cm^2.s^{-1}$ and 10.50–51.10 nm and a PL emission centered at $\lambda = 650$ μm. Implying that for the mixture, the thermal conduction is made by the phonons vibrations, it can be used as a thermoinsultor, a thermocondensor material or a red emitter device.

Acknowledgment

This work was supported by Imam Abdulrahman Bin Faisal University, Saudi Arabia through Grant NO. 2015189.

Appendix A. Supplementary data

Supplementary data associated with this article can be found, in the online version, at https://doi.org/10.1016/j.rinp.2017.12.048.

References

[1] Barrer RM. Zeolites and clay minerals as sorbents and molecular sieves. London: Academic Press; 1998.
[2] Barrer RM, Beaumont R, Colella C. Chemistry of soil minerals, Part XIV, Action of some basic solution on metakaolinite and kaolinite. J Chem Soc Dalton Trans 1974:934.
[3] Ruiz R, Banco C, Pesquera C, Gonzalez F, Benito I, Lopez JL. Zeolitization of a bentonite and its application to the removal of ammonium ion from waste water. Appl Clay Sci 1997;12:73.
[4] Baccouche A, Srasra E, Maaoui ME. Preparation of Na–P1 and sodalite octahydrate zeolites from interstratified illite-smectite. Appl Clay Sci 1998;13:255–73.
[5] Gualtieri AF. Synthesis of sodium zeolites from a natural halloysite. Phys Chem Miner 2001;28:719.
[6] Boukadir D, Bettahar N, Derriche Z. Synthesis of zeolites 4A and HS from natural materials. Annu Chim Sci Mat 2002;27:1.
[7] Querol X, Moreno N, Umana JC, Alastuey A, Hernandez E. Synthesis of zeolites from coal fly ash: an overview. Int J Coal Geol 2000;50:413.
[8] Yang GCC, Yang T. Synthesis of zeolites from municipal incinerator fly ash. J Hazard Mater 1998;6:275.
[9] Wajima T, Kuzawa K, Ishimoto H, Tamada O, Nishiyama T. The synthesis of zeolite-P, Linde type A, and hydroxysodalite zeolites from paper sludge ash at low temperature (80 °C): optimal ash-leaching condition for zeolite synthesis. Am Miner 2004;89:1694.
[10] Olenina ZK, Moreva NP, Yasyan YuP, Adzhiev AYu. Chem Technol Fuels Oils 1991;27:214 (English Trans Khimiya I Tekhnologiya Topliv I Masel).
[11] Harben PW, Bates RL. Industrial Minerals: Geology and World Deposits Metal Bulletin, London;1990. p. 302–6.
[12] Tonucci RJ, Justus BL, Campillo AJ, Ford CE. Nanochannel Array Glass Sci 1992;258:783.
[13] Whitney TW, Jiang JS, Searson PC, Chien CL. Fabrication and magnetic properties of arrays of metallic nanowires. Science 1993;261:1316.
[14] Nielsch K, Wehrspohn RB, Barthel J, Kirschner J, Gosele U, Fischer SF, Kronmuller H. Hexagonally ordered 100 nm period nickel nanowire arrays. Appl Phys. Lett. 2001;79:1360.
[15] Karmhag R, Tesfamichael T, Wackelgard E, Niklasson GA. Oxidation kinetics of nickel particles: comparison between free particles and particles in an oxide matrix. Sol Energy 2000;68:329–33.
[16] Che G, Lakshmi BB, Fisher ER, Martin CR. Carbon nanotubule membranes for electrochemical energy storage and production. Nature 1998;393:346–9.
[17] Che G, Lakshmi BB, Martin CR, Fisher ER, Ruoff RS. Chemical vapor deposition based synthesis of carbon nanotubes and nanofibers using a template method. Chem Mater 1998;10:260–7.
[18] Zhang ZB, Gekhtman D, Dresselhaus MS, Ying JY. Processing and characterization of single-crystalline ultrafine bismuth nanowires. Chem Mater 1999;11:1659–65.
[19] Sauer G, Brehm G, Schneider S, Nielsch K, Wehrspohn RB, Choi J, Hofmeister H, Gosele UJ. Highly ordered monocrystalline silver nanowire arrays. J Appl Phys 2002;91:3243.
[20] Somayajulu PS, Ghosh PS, Banerjee J, Babu KLNC, Arya A. Experimental and molecular dynamics study of thermo-physical and transport properties of ThO2-5 wt%CeO2 mixed oxides. J Nucl Mater 2015;467:644–59.
[21] Biçen M, Apohan NK, Karatas S, Dumludag F, Güngor A. The Effect of surface modification of zeolite 4a on the physical and electrical properties of copolyimide hybrid films. Microporous Mesoporous Mater 2015;218:79–87.
[22] Jakubinek MB, Zhan BZ, Anne M. White temperature-dependent thermal conductivity of powdered zeolite NaX. Microporous Mesoporous Mater 2007;103:108–12.
[23] Ghrib T, Gaied I, Yacoubi N. Investigation of thermal properties of steel undergoing heat treatment by the photothermal deflection technique: correlation with mechanical properties. Nova publishers; 2010. p. 146.
[24] Ghrib T. Structural, optical and thermal properties of nanoporous aluminum. Thermochim Acta 2015;599:57–62.
[25] Ghrib T, Al-Otaibi AL, Almessiere MA, Assaker IB, Chtourou R. High thermoelectric figure of merit of Ag8SnS6 component prepared by electrodeposition technique. Chin Phys Lett 2015;32:127402.
[26] Ghrib T, Al-Otaibi AL, Almessiere MA, Ashahri A, Masoudi I. Structural, optical and thermal properties of the Ce doped YAG synthesized by solid state reaction method. Thermochim Acta 2017;654:35–9.

[27] Jeon PS, Kim JH, Kim HJ, Yoo J. Thermal conductivity measurement of anisotropic material using photothermal deflection method. Thermochimi Acta 2008;477:32–7.
[28] Meftah M, Oueslati W, Ben Haj Amara A. Synthesis of zeolites A and P from 1:1 and HS from 2:1 clays. Mater Sci Eng 2010;13. 012019.
[29] Reed TB, Breck DW. Crystalline zeolites II, crystal structure of synthetic zeolite, type A. Am Chem Soc 1956;78:5972.
[30] Gramlich V, Meier WM. The crystal structure of hydrated NaA: a detailed refinement of a pseudosymmetric zeolite structure. Z Kristallogr 1971;133:134–49.
[31] Simmen A, Patarin J, Baerlocher. Ch Proc. 9th Int. Zeolite Conf. p. 433.
[32] Zivica V, Palou M, Ifka T. High strength metakaolin based geopolymer. Build Res J 2012;60.
[33] Pham HV, Maruoka D, Nanko M. Influences of Al2O3 grain size on high-temperature oxidation of nano-Ni/Al2O3 composites. J Asian Ceram Soc 2016;4(1):120–3.
[34] Murashov Vladimir V, White Mary Anne. Thermal properties of zeolites: effective thermal conductivity of dehydrated powdered zeolite 4A. Mater Chem Phys 2002;75:178–80.
[35] Pelissari Pedro IBGB, Angélico Ricardo A, Salvini Vânia R, Vivaldini Diogo O, Pandolfelli Victor C. Analysis and modeling of the pore size effect on the thermal conductivity of alumina foams for high temperature applications. Ceram Int 2017;43:13356–63.
[36] Fukushima Manabu, Yoshizawa Yu-ichi. Fabrication and morphology control of highly porous mullite thermal insulators prepared by gelation freezing route. J Eur Ceram Soc 2016;36:2947–53.
[37] Singh D, Murthy JY, Fisher TS. Effect of phonon dispersion on thermal conduction across Si/Ge interfaces, School of Mechanical Engineering and Birck Nanotechnology Center. Purdue University. West Lafayette, IN -47907, USA.